

# Higher-order radiative corrections for $b\bar{b} \rightarrow H^- W^+$

Nikolaos Kidonakis

*Department of Physics, Kennesaw State University,  
Kennesaw, GA 30144, USA*

## Abstract

I present higher-order radiative corrections from collinear and soft gluon emission for the associated production of a charged Higgs boson with a  $W$  boson. The calculation uses expressions from resummation at next-to-leading-logarithm accuracy. From the resummed cross section I derive approximate next-to-next-to-leading order (aNNLO) cross sections for the process  $b\bar{b} \rightarrow H^- W^+$  at LHC energies. The transverse-momentum and rapidity distributions of the charged Higgs boson are also calculated at aNNLO.

## 1 Introduction

Higgs bosons play a central role in both the Standard Model and in searches for new physics. Two-Higgs-doublet models in new physics scenarios, such as the Minimal Supersymmetric Standard Model, involve charged Higgs bosons in addition to neutral ones. One of the Higgs doublets gives mass to up-type fermions while the other to down-type fermions, with the ratio of the vacuum expectation values for the two doublets denoted by  $\tan\beta$ . Two charged Higgs bosons,  $H^+$  and  $H^-$ , appear in such models.

An important charged Higgs production process at LHC energies is the associated production of a charged Higgs boson with a  $W$  boson, which may proceed via the partonic process  $b\bar{b} \rightarrow H^- W^+$  or  $b\bar{b} \rightarrow H^+ W^-$ . This process was studied in Refs. [1–18] and various kinds of radiative corrections were calculated in those works.

An important set of higher-order corrections is due to soft-gluon emission, dominant near partonic threshold; another is due to collinear gluon emission. These corrections can in principle be resummed, and the resummation formalism can be used to construct approximate higher-order results.

In this paper I present a first study of collinear and soft-gluon resummation for the associated production of a charged Higgs boson with a  $W$  boson via  $b$ -quark annihilation. Since the charged Higgs is presumably very massive, its possible production at the LHC would be a near-threshold process.

I employ the resummation formalism that has been used for several related processes, including charged Higgs production in association with a top quark [19, 20], neutral Higgs production via  $b\bar{b}$  annihilation [21],  $W$  or  $Z$  production at large transverse momentum [22], top-quark production in association with a  $W$  boson [20, 23, 24], and top-antitop pair production [23, 25].

In the next section we discuss collinear and soft-gluon corrections and present their resummation. Using the expansion of the resummed cross section at next-to-leading order (NLO) and next-to-next-to-leading order (NNLO), we derive approximate NLO (aNNLO) and approximate NNLO (aNNLO) cross sections. In Section 3 we present results for  $H^- W^+$  total cross sections at LHC energies. In Section 4 we present results for the charged Higgs transverse momentum and rapidity distribution in this process. We conclude in Section 5.

## 2 Collinear and soft-gluon resummation for $b\bar{b} \rightarrow H^-W^+$

For the process  $b\bar{b} \rightarrow H^-W^+$ , involving bottom quarks in the initial state, we assign the momenta

$$b(p_1) + \bar{b}(p_2) \rightarrow H^-(p_3) + W^+(p_4), \quad (2.1)$$

and define the kinematical variables  $s = (p_1 + p_2)^2$ ,  $t = (p_1 - p_3)^2$ ,  $t_1 = t - m_H^2$ ,  $t_2 = t - m_W^2$ ,  $u = (p_2 - p_3)^2$ ,  $u_1 = u - m_H^2$ , and  $u_2 = u - m_W^2$ , where  $m_H$  is the charged Higgs mass and  $m_W$  is the  $W$ -boson mass while the  $b$ -quark mass is taken to be 0. We also define the variable  $s_4 = s + t_1 + u_2$ , which measures distance from partonic threshold where there is no energy for additional emission; however, even when  $s_4 = 0$  the charged Higgs boson and the  $W$  boson are not constrained to be produced at rest. We note that identical considerations apply to  $H^+W^-$  production.

Radiative corrections, including collinear and soft-gluon corrections, appear at each order in the perturbative expansion of the cross section. The soft-gluon terms are plus distributions of logarithms of  $s_4$ ,  $[(\ln^k(s_4/m_H^2))/s_4]_+$ , with  $k$  an integer ranging from 0 to  $2n - 1$  for the  $n$ th order corrections in the strong coupling,  $\alpha_s$ .

The plus distributions are defined by their integrals with functions  $f$ , which in our case involve perturbative coefficients and parton distribution functions (pdf) as discussed later, as

$$\begin{aligned} \int_0^{s_4^{max}} ds_4 \left[ \frac{\ln^k(s_4/m_H^2)}{s_4} \right]_+ f(s_4) &= \int_0^{s_4^{max}} ds_4 \frac{\ln^k(s_4/m_H^2)}{s_4} [f(s_4) - f(0)] \\ &+ \frac{1}{k+1} \ln^{k+1} \left( \frac{s_4^{max}}{m_H^2} \right) f(0). \end{aligned} \quad (2.2)$$

In addition, further logarithmic terms of the form  $(1/m_H^2) \ln^k(s_4/m_H^2)$ , of collinear origin, also appear in the perturbative expansion. These collinear terms are fully known only at leading logarithmic accuracy.

Resummation of collinear and soft-gluon contributions follows from the factorization of the cross section into various functions that describe collinear and soft emission in the partonic process. Taking moments of the partonic scattering cross section,  $\hat{\sigma}(N) = \int (ds_4/s) e^{-Ns_4/s} \hat{\sigma}(s_4)$ , with  $N$  the moment variable, we write a factorized expression in  $4 - \epsilon$  dimensions:

$$\hat{\sigma}^{H^-W^+}(N, \epsilon) = \left( \prod_{i=b, \bar{b}} J_i(N, \mu, \epsilon) \right) H^{H^-W^+}(\alpha_s(\mu)) S^{H^-W^+} \left( \frac{m_H}{N\mu}, \alpha_s(\mu) \right) \quad (2.3)$$

where  $\mu$  is the scale,  $J_i$  are jet functions that describe soft and collinear emission from the incoming  $b$  and  $\bar{b}$  quarks,  $H^{H^-W^+}$  is the hard-scattering function, and  $S^{H^-W^+}$  is the soft-gluon function for non-collinear soft-gluon emission. The lowest-order cross section is given by the product of the lowest-order hard and soft functions.

The soft function  $S^{H^-W^+}$  requires renormalization and its  $N$ -dependence can be resummed via renormalization group evolution. Thus,  $S^{H^-W^+}$  satisfies the renormalization group equation

$$\left( \mu \frac{\partial}{\partial \mu} + \beta(g_s, \epsilon) \frac{\partial}{\partial g_s} \right) S^{H^-W^+} = -2 S^{H^-W^+} \Gamma_S^{H^-W^+} \quad (2.4)$$

where  $g_s^2 = 4\pi\alpha_s$ ;  $\beta(g_s, \epsilon) = -g_s\epsilon/2 + \beta(g_s)$  with  $\beta(g_s)$  the QCD beta function; and  $\Gamma_S^{H^-W^+}$  is the soft anomalous dimension that controls the evolution of the soft-gluon function  $S^{H^-W^+}$ .

The evolution of the soft and jet functions provides resummed expressions for the cross section [19–25]. For  $H^-W^+$  production the resummed partonic cross section in moment space is given by

$$\begin{aligned} \hat{\sigma}_{\text{res}}^{H^-W^+}(N) &= \exp \left[ \sum_{i=b, \bar{b}} E_i(N_i) \right] H^{H^-W^+}(\alpha_s(\sqrt{s})) S^{H^-W^+}(\alpha_s(\sqrt{s}/\tilde{N}')) \\ &\times \exp \left[ 2 \int_{\sqrt{s}}^{\sqrt{s}/\tilde{N}'} \frac{d\mu}{\mu} \Gamma_S^{H^-W^+}(\alpha_s(\mu)) \right]. \end{aligned} \quad (2.5)$$

The first exponent [26, 27] in Eq. (2.5) resums soft and collinear corrections from the incoming  $b$  and  $\bar{b}$  quarks and is well known (see [20] for details). The specific forms for the expressions for the individual terms depend on the gauge, although the overall result for the resummed cross section of course does not. In Feynman gauge the one-loop soft anomalous dimension for  $b\bar{b} \rightarrow H^-W^+$  vanishes; in axial gauge it is  $(\alpha_s/\pi)C_F$ , where  $C_F = (N_c^2 - 1)/(2N_c)$  with  $N_c = 3$  the number of colors. We calculate the soft-gluon corrections at next-to-leading-logarithm accuracy. However, as mentioned previously, only the leading collinear corrections are fully known.

We expand the resummed cross section, Eq. (2.5), in  $\alpha_s$ , and then we invert to momentum space and provide results through second order for the soft-gluon corrections.

The NLO collinear and soft-gluon corrections from the resummation are

$$\begin{aligned} \frac{d^2\hat{\sigma}^{(1)}}{dt du} &= \frac{\pi\alpha^2 m_t^4 \cot^2 \beta}{48 \sin^4 \theta_W m_W^4 s^2 t_1^2} (m_W^2 s + t_2 u_2) \frac{\alpha_s(\mu_R)}{\pi} C_F \left\{ -\frac{4}{m_H^2} \ln \left( \frac{s_4}{m_H^2} \right) \right. \\ &+ 4 \left[ \frac{\ln(s_4/m_H^2)}{s_4} \right]_+ - 2 \left[ \ln \left( \frac{t_2 u_2}{m_H^4} \right) + \ln \left( \frac{\mu_F^2}{s} \right) \right] \left[ \frac{1}{s_4} \right]_+ \\ &\left. + \left[ \ln \left( \frac{t_2 u_2}{m_H^4} \right) - \frac{3}{2} \right] \ln \left( \frac{\mu_F^2}{m_H^2} \right) \delta(s_4) \right\} \end{aligned} \quad (2.6)$$

where  $\alpha = e^2/(4\pi)$ ,  $\theta_W$  is the weak mixing angle,  $\mu_R$  is the renormalization scale, and  $\mu_F$  is the factorization scale.

The NNLO collinear and soft-gluon corrections from the resummation are

$$\begin{aligned} \frac{d^2\hat{\sigma}^{(2)}}{dt du} &= \frac{\pi\alpha^2 m_t^4 \cot^2 \beta}{48 \sin^4 \theta_W m_W^4 s^2 t_1^2} (m_W^2 s + t_2 u_2) \frac{\alpha_s^2(\mu_R)}{\pi^2} C_F \\ &\times \left\{ -8C_F \frac{1}{m_H^2} \ln^3 \left( \frac{s_4}{m_H^2} \right) + 8C_F \left[ \frac{\ln^3(s_4/m_H^2)}{s_4} \right]_+ \right. \\ &+ \left[ -12C_F \left( \ln \left( \frac{t_2 u_2}{m_H^4} \right) + \ln \left( \frac{\mu_F^2}{s} \right) \right) - \frac{11}{3}C_A + \frac{2}{3}n_f \right] \left[ \frac{\ln^2(s_4/m_H^2)}{s_4} \right]_+ \\ &\left. + \left[ 4C_F \ln^2 \left( \frac{\mu_F^2}{m_H^2} \right) + C_F \left( 12 \ln \left( \frac{t_2 u_2}{m_H^4} \right) + 8 \ln \left( \frac{m_H^2}{s} \right) - 6 \right) \ln \left( \frac{\mu_F^2}{m_H^2} \right) \right] \right\} \end{aligned}$$

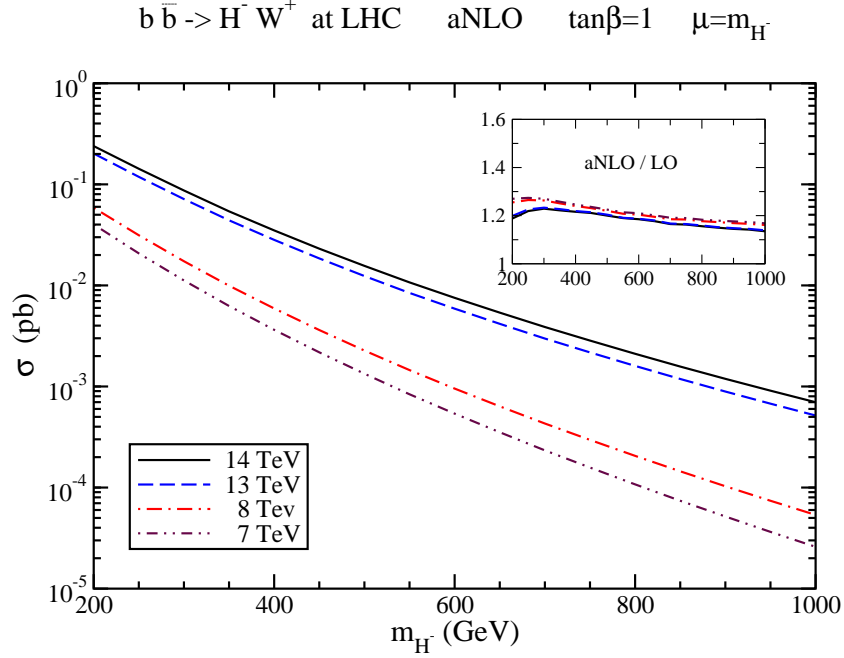


Figure 1: The aNLO cross sections for  $b\bar{b} \rightarrow H^- W^+$  at the LHC with  $\sqrt{S} = 7, 8, 13$ , and 14 TeV.

$$\begin{aligned}
& + \left( \frac{11}{3} C_A - \frac{2}{3} n_f \right) \ln \left( \frac{\mu_R^2}{m_H^2} \right) \left[ \frac{\ln(s_4/m_H^2)}{s_4} \right]_+ \\
& + \left[ \left( -2C_F \ln \left( \frac{t_2 u_2}{m_H^4} \right) + 3C_F + \frac{11}{12} C_A - \frac{n_f}{6} \right) \ln^2 \left( \frac{\mu_F^2}{m_H^2} \right) \right. \\
& \quad \left. - \left( \frac{11}{6} C_A - \frac{n_f}{3} \right) \ln \left( \frac{\mu_F^2}{m_H^2} \right) \ln \left( \frac{\mu_R^2}{m_H^2} \right) \right] \left[ \frac{1}{s_4} \right]_+ \Big\} \quad (2.7)
\end{aligned}$$

where  $C_A = N_c$ , and  $n_f = 5$  is the number of light-quark flavors.

Equation (2.7) can be written more compactly as

$$\frac{d^2 \hat{\sigma}^{(2)}}{dt du} = F_{LO} \frac{\alpha_s^2}{\pi^2} \left\{ -C_3^{(2)} \frac{1}{m_H^2} \ln^3 \left( \frac{s_4}{m_H^2} \right) + \sum_{k=0}^3 C_k^{(2)} \left[ \frac{\ln^k(s_4/m_H^2)}{s_4} \right]_+ \right\} \quad (2.8)$$

where  $F_{LO}$  denotes the overall leading-order factor and the  $C_k^{(2)}$  are coefficients of the logarithms, and they can be read off by comparing Eq. (2.8) with Eq. (2.7). This compact form for the aNNLO corrections will be useful in the next section.

### 3 aNNLO total cross sections for $H^- W^+$ production

We consider proton-proton collisions with momenta  $p(p_A) + p(p_B) \rightarrow H^-(p_3) + W^+(p_4)$ . In analogy to the partonic variables defined in Section 2, we define the hadronic kinematical

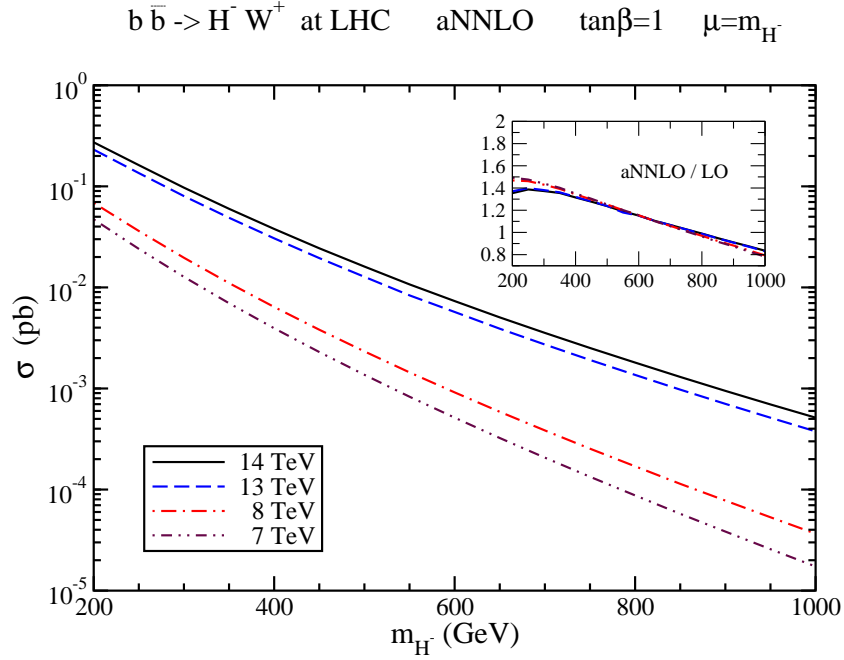


Figure 2: The aNNLO cross sections for  $b\bar{b} \rightarrow H^- W^+$  at the LHC with  $\sqrt{S} = 7, 8, 13$ , and 14 TeV.

variables  $S = (p_A + p_B)^2$ ,  $T = (p_A - p_3)^2$ ,  $T_1 = T - m_H^2$ ,  $T_2 = T - m_W^2$ ,  $U = (p_B - p_3)^2$ , and  $U_1 = U - m_H^2$ . The hadronic variables are related to the partonic variables via  $p_1 = x_1 p_A$  and  $p_2 = x_2 p_B$ , where  $x_1$  and  $x_2$  are the fractions of the momentum carried by the partons in protons  $A$  and  $B$ , respectively.

The hadronic total cross section can be written as

$$\sigma^{H^- W^+} = \int_{T_{min}}^{T_{max}} dT \int_{U_{min}}^{U_{max}} dU \int_{x_2^{min}}^1 dx_2 \int_0^{s_4^{max}} ds_4 \frac{x_1 x_2}{x_2 S + T_1} \phi(x_1) \phi(x_2) \frac{d^2 \hat{\sigma}}{dt du} \quad (3.1)$$

where the  $\phi$  denote the pdf;  $x_1 = (s_4 - m_H^2 + m_W^2 - x_2 U_1) / (x_2 S + T_1)$ ;  $T_{min}^{max} = -(1/2)(S - m_H^2 - m_W^2) \pm (1/2)[(S - m_H^2 - m_W^2)^2 - 4m_H^2 m_W^2]^{1/2}$ ;  $U_{max} = m_H^2 + S m_H^2 / T_1$  and  $U_{min} = -S - T_1 + m_W^2$ ;  $x_2^{min} = -T_2 / (S + U_1)$ ; and  $s_4^{max} = x_2(S + U_1) + T_2$ .

Specifically, using the properties of plus distributions, Eq. (2.2), and the compact form of Eq. (2.8), the aNNLO corrections to the total cross section, Eq. (3.1), can be written as

$$\begin{aligned} \sigma_{H^- W^+}^{(2)} &= \frac{\alpha_s^2}{\pi^2} \int_{T_{min}}^{T_{max}} dT \int_{U_{min}}^{U_{max}} dU \int_{x_2^{min}}^1 dx_2 \phi(x_2) \frac{x_2}{x_2 S + T_1} \\ &\times \left\{ - \int_0^{s_4^{max}} ds_4 \frac{1}{m_H^2} \ln^3 \left( \frac{s_4}{m_H^2} \right) F_{LO} C_3^{(2)} x_1 \phi(x_1) \right. \\ &\quad \left. + \sum_{k=0}^3 \left[ \int_0^{s_4^{max}} ds_4 \frac{1}{s_4} \ln^k \left( \frac{s_4}{m_H^2} \right) (F_{LO} C_k^{(2)} x_1 \phi(x_1) - F_{LO}^{el} C_k^{(2)el} x_1^{el} \phi(x_1^{el})) \right] \right\} \end{aligned}$$

$$+ \frac{1}{k+1} \ln^{k+1} \left( \frac{s_4^{max}}{m_H^2} \right) F_{LO}^{el} C_k^{(2)el} x_1^{el} \phi(x_1^{el}) \Big] \Big\} . \quad (3.2)$$

where  $x_1^{el}$ ,  $F_{LO}^{el}$ , and  $C_k^{(2)el}$  denote the elastic variables, i.e. these quantities with  $s_4 = 0$ .

We now present results for the total  $H^-W^+$  cross section at LHC energies using MMHT2014 NNLO pdf [28]. For convenience we set  $\tan \beta = 1$  but it is easy to rescale the results for any value of  $\tan \beta$ .

In Fig. 1 we plot the aNLO cross sections for  $b\bar{b} \rightarrow H^-W^+$  in proton-proton collisions at the LHC versus charged Higgs mass for energies of 7, 8, 13, and 14 TeV. The inset plot shows the  $K$ -factors, i.e. the aNLO/LO ratios. The corrections are clearly very significant for all LHC energies.

In Fig. 2 we plot the aNNLO cross sections for  $b\bar{b} \rightarrow H^-W^+$  versus charged Higgs mass for LHC energies of 7, 8, 13, and 14 TeV. The inset plot shows the aNNLO/LO  $K$ -factors.

In both figures we observe an order of magnitude or so increase in the cross section at 13 and 14 TeV relative to 7 and 8 TeV. We also observe a large dependence of the cross section on the charged Higgs mass at each energy, with three orders of magnitude or more variation between 200 and 1000 GeV.

Theoretical uncertainties arise from scale variation as well as from pdf uncertainties. Scale variation by a factor of 2 around the central scale  $\mu = m_H$  produces a moderate uncertainty,  $\pm 15\%$  at 13 TeV LHC energy for a 500 GeV charged Higgs, with similar numbers at other energies. The uncertainties from the pdf are smaller,  $\pm 5\%$  at 13 TeV for a 500 GeV charged Higgs.

We note that results using other pdf sets are very similar. If one uses the CT14 NNLO pdf [29] the results are essentially the same.

## 4 aNNLO charged Higgs $p_T$ and rapidity distributions

We continue with the charged Higgs  $p_T$  and rapidity distributions. The charged Higgs  $p_T$  distribution is given by

$$\frac{d\sigma}{dp_T} = 2 p_T \int_{Y^{min}}^{Y^{max}} dY \int_{x_2^{min}}^1 dx_2 \int_0^{s_4^{max}} ds_4 \frac{x_1 x_2 S}{x_2 S + T_1} \phi(x_1) \phi(x_2) \frac{d^2 \hat{\sigma}}{dt du} \quad (4.1)$$

where  $T_1 = -\sqrt{S} (m_H^2 + p_T^2)^{1/2} e^{-Y}$ ,  $U_1 = -\sqrt{S} (m_H^2 + p_T^2)^{1/2} e^Y$ ,  $Y_{min}^{max} = \pm (1/2) \ln[(1 + \beta_T)/(1 - \beta_T)]$  with  $\beta_T = [1 - 4(m_H^2 + p_T^2)S/(S + m_H^2 - m_W^2)^2]^{1/2}$ , and the other quantities are defined in Section 3. We note that the total cross section can also be calculated by integrating the  $p_T$  distribution,  $d\sigma/dp_T$ , over  $p_T$  from 0 to  $p_T^{max} = [(S - m_H^2 - m_W^2)^2 - 4m_H^2 m_W^2]^{1/2}/(2\sqrt{S})$ , and we have checked for consistency that we get the same numerical results as in Section 3.

In Fig. 3 we plot the aNNLO  $p_T$  distributions,  $d\sigma/dp_T$ , of the charged Higgs boson with mass 200 GeV for LHC energies of 7, 8, 13, and 14 TeV. The inset plot shows the aNNLO/LO  $K$ -factors. The corrections are large, around 50%, for much of the  $p_T$  range shown. The distributions peak at a  $p_T$  value of around 65 GeV for this mass choice.

In Fig. 4 we plot the corresponding aNNLO  $p_T$  distributions of the charged Higgs boson with mass 500 GeV. The inset plot shows the aNNLO/LO  $K$ -factors and, again, the corrections are large. The distributions now peak at a higher  $p_T$  value of around 110 GeV.

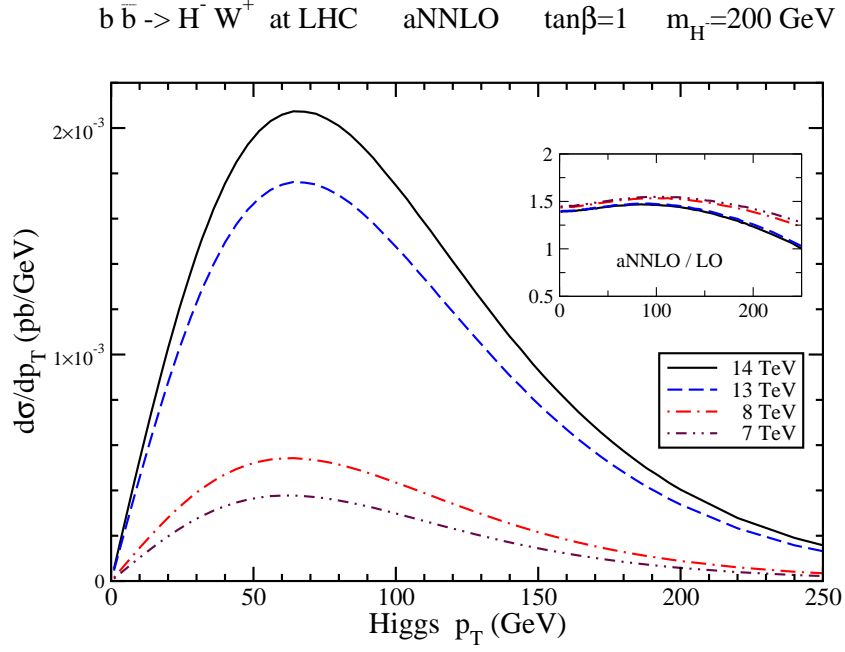


Figure 3: The aNNLO charged Higgs  $p_T$  distributions for  $b\bar{b} \rightarrow H^- W^+$  at the LHC with  $\sqrt{S} = 7, 8, 13$ , and 14 TeV, and  $m_H = 200$  GeV.

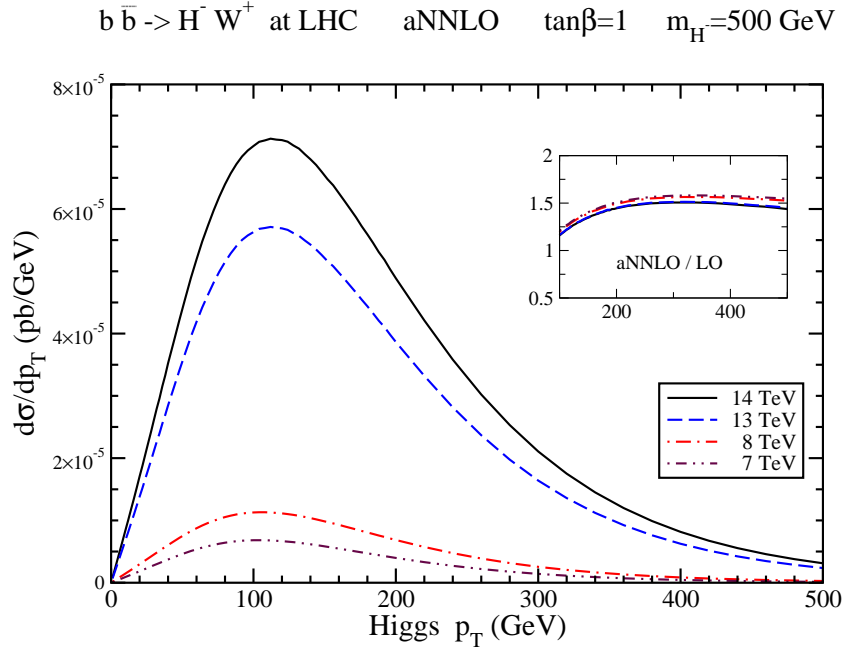


Figure 4: The aNNLO charged Higgs  $p_T$  distributions for  $b\bar{b} \rightarrow H^- W^+$  at the LHC with  $\sqrt{S} = 7, 8, 13$ , and 14 TeV, and  $m_H = 500$  GeV.

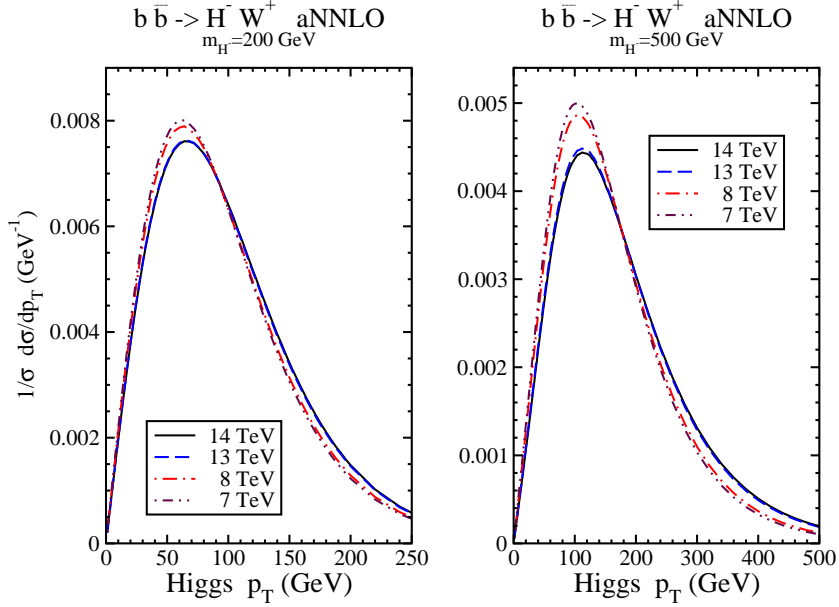


Figure 5: The aNNLO charged Higgs normalized  $p_T$  distributions for  $b\bar{b} \rightarrow H^- W^+$  at the LHC with  $\sqrt{S} = 7, 8, 13$ , and  $14$  TeV, and  $m_H = 200$  GeV (left) and  $500$  GeV (right).

It is useful to also study normalized distributions since normalization removes the dependence on  $\tan\beta$  and it minimizes the dependence on the choice of pdf. Such normalized distributions are also often favored in experimental studies and comparisons with theory.

In Fig. 5 we plot the aNNLO normalized  $p_T$  distributions,  $(1/\sigma)d\sigma/dp_T$ , of the charged Higgs boson with mass  $200$  GeV (left plot) and  $500$  GeV (right plot) for LHC energies of  $7, 8, 13$ , and  $14$  TeV. The shape of the normalized  $p_T$  distributions depends on the energy, as expected, with higher peaks at lower energies. We also observe that the peaks are lower for a  $500$  GeV mass than for  $200$  GeV.

The charged-Higgs rapidity,  $Y$ , distribution is given by

$$\frac{d\sigma}{dY} = \int_0^{p_T^{max}} 2 p_T dp_T \int_{x_2^{min}}^1 dx_2 \int_0^{s_4^{max}} ds_4 \frac{x_1 x_2 S}{x_2 S + T_1} \phi(x_1) \phi(x_2) \frac{d^2\hat{\sigma}}{dt du} \quad (4.2)$$

where  $p_T^{max} = ((S + m_H^2 - m_W^2)^2 / (4S \cosh^2 Y) - m_H^2)^{1/2}$  and the rest of the quantities are defined as before. We again note that the total cross section can also be obtained by integrating the rapidity distribution,  $d\sigma/dY$ , over rapidity with limits  $Y_{min}^{max} = \pm(1/2) \ln[(1 + \beta)/(1 - \beta)]$  where  $\beta = (1 - 4m_H^2/S)^{1/2}$ , and again we have checked for consistency that we get the same numerical results as in Section 3.

In Fig. 6 we plot the aNNLO rapidity distributions,  $d\sigma/d|Y|$ , of the charged Higgs boson with mass  $200$  GeV for LHC energies of  $7, 8, 13$ , and  $14$  TeV. The inset plot shows the aNNLO/LO  $K$ -factors. The corrections are quite large, especially at lower LHC energies, and grow at larger values of charged Higgs rapidity.

In Fig. 7 we plot the corresponding aNNLO rapidity distributions of the charged Higgs boson with mass  $500$  GeV. The aNNLO/LO  $K$ -factors are again shown in the inset plot. We



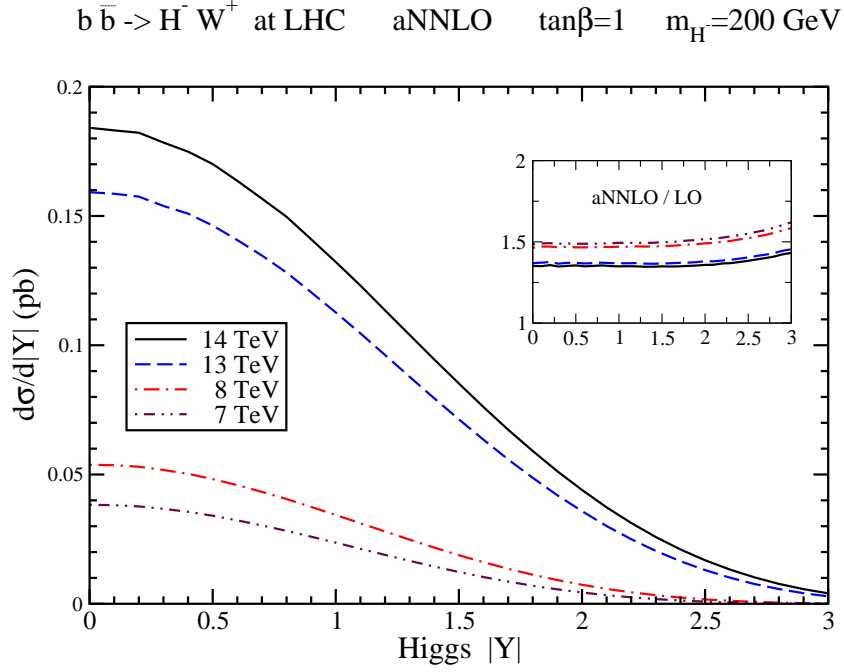


Figure 6: The aNNLO charged Higgs rapidity distributions for  $b\bar{b} \rightarrow H^- W^+$  at the LHC with  $\sqrt{S} = 7, 8, 13$ , and  $14$  TeV, and  $m_H = 200$  GeV.

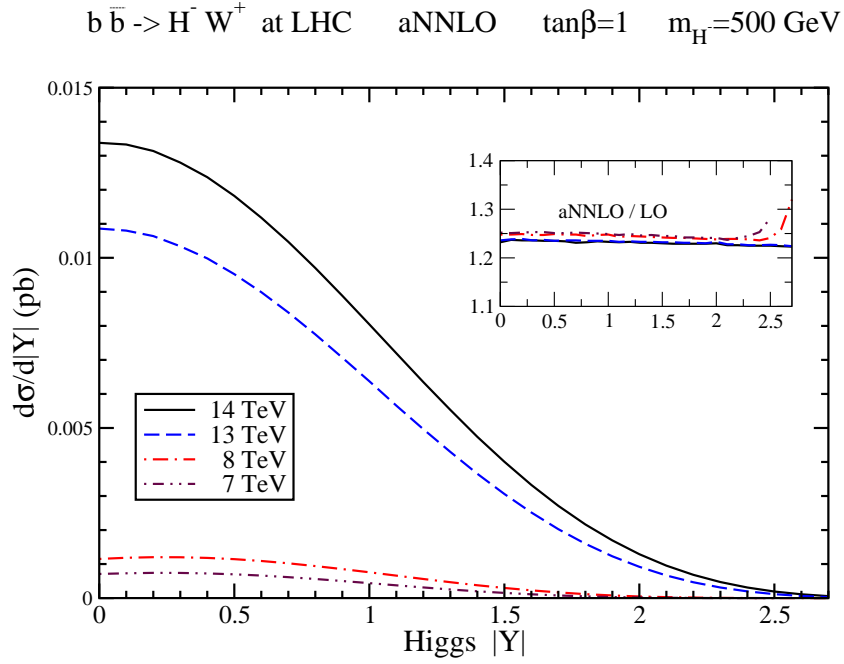


Figure 7: The aNNLO charged Higgs rapidity distributions for  $b\bar{b} \rightarrow H^- W^+$  at the LHC with  $\sqrt{S} = 7, 8, 13$ , and  $14$  TeV, and  $m_H = 500$  GeV.

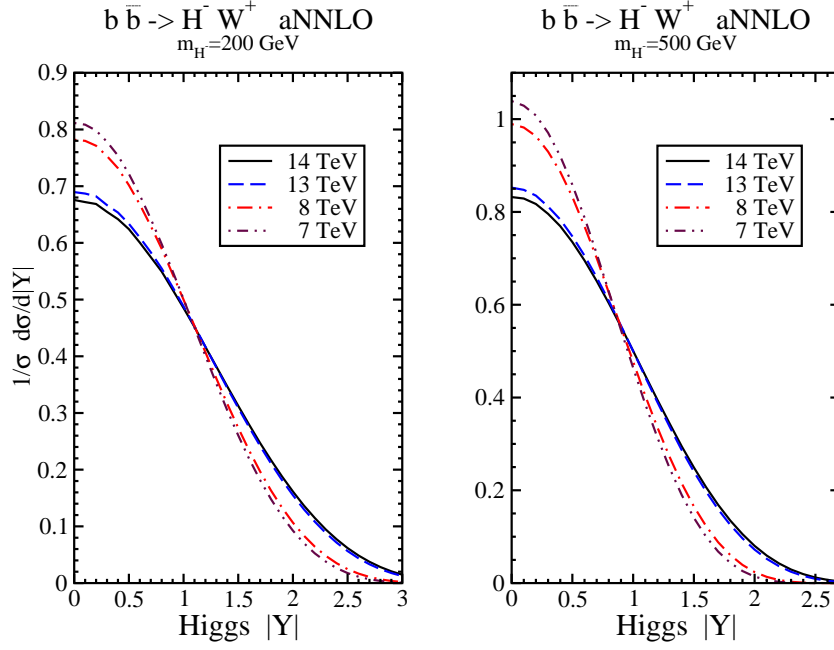


Figure 8: The aNNLO charged Higgs normalized rapidity distributions for  $b\bar{b} \rightarrow H^- W^+$  at the LHC with  $\sqrt{S} = 7, 8, 13$ , and  $14$  TeV, and  $m_H = 200$  GeV (left) and  $500$  GeV (right).

observe that the 7 and 8 TeV  $K$ -factors increase rapidly at larger values of rapidity.

Finally, in Fig. 8 we plot the aNNLO normalized rapidity distributions,  $(1/\sigma)d\sigma/d|Y|$ , of the charged Higgs boson with mass  $200$  GeV (left plot) and  $500$  GeV (right plot) for LHC energies of  $7, 8, 13$ , and  $14$  TeV. For a given charged Higgs mass the normalized rapidity distributions at lower energies have higher peaks at central rapidity with corresponding smaller values at large  $|Y|$ , as expected. The fall of the distributions with increasing  $|Y|$  is sharper for  $m = 500$  GeV than for  $200$  GeV at all LHC energies.

## 5 Conclusions

The cross sections for the associated production of a charged Higgs boson with a  $W$  boson, via  $b\bar{b} \rightarrow H^- W^+$ , receive sizable contributions from collinear and soft gluon corrections. These radiative contributions have been resummed, and approximate NNLO double-differential cross sections were derived. Numerical predictions were provided for the total cross section for  $H^- W^+$  production at LHC energies as well as for the  $p_T$  and rapidity distributions of the charged Higgs boson. The higher-order corrections are significant and they enhance the total cross section and differential distributions for  $H^- W^+$  production at the LHC.

# Acknowledgements

This material is based upon work supported by the National Science Foundation under Grant No. PHY 1519606.

# References

- [1] D.A. Dicus, J.L. Hewett, C. Kao, and T.G. Rizzo, Phys. Rev. D **40**, 787 (1989).
- [2] D.A. Dicus and C. Kao, Phys. Rev. D **41**, 832 (1990).
- [3] Y.S. Yang, C.S. Li, L.G. Jin, and S.H. Zhu, Phys. Rev. D **62**, 095012 (2000) [hep-ph/0004248].
- [4] F. Zhou, W.-G. Ma, Y. Jiang, L. Han, and L.-H. Wan, Phys. Rev. D **63**, 015002 (2001).
- [5] O. Brein, W. Hollik, and S. Kanemura, Phys. Rev. D **63**, 095001 (2001) [hep-ph/0008308].
- [6] W. Hollik and S.-H. Zhu, Phys. Rev. D **65**, 075015 (2002) [hep-ph/0109103].
- [7] E. Asakawa, O. Brein, and S. Kanemura, Phys. Rev. D **72**, 055017 (2005) [hep-ph/0506249].
- [8] J. Zhao, C.S. Li, and Q. Li, Phys. Rev. D **72**, 114008 (2005) [hep-ph/0509369].
- [9] D. Eriksson, S. Hesselbach, and J. Rathsman, Eur. Phys. J. C **53**, 267 (2008) [hep-ph/0612198]; J. Phys. Conf. Ser. **110**, 072008 (2008) [arXiv:0710.0526].
- [10] J. Gao, C.S. Li, and Z. Li, Phys. Rev. D **77**, 014032 (2008) [arXiv:0710.0826 [hep-ph]].
- [11] M. Hashemi, Phys. Rev. D **83**, 055004 (2011) [arXiv:1008.3785 [hep-ph]].
- [12] S.-S. Bao, Y. Tang, and Y.-L. Wu, Phys. Rev. D **83**, 075006 (2011) [arXiv:1011.1409 [hep-ph]].
- [13] T.N. Dao, W. Hollik, and D.N. Le, Phys. Rev. D **83**, 075003 (2011) [arXiv:1011.4820 [hep-ph]].
- [14] M. Aoki, R. Guedes, S. Kanemura, S. Moretti, R. Santos, and K. Yagyu, Phys. Rev. D **84**, 055028 (2011) [arXiv:1104.3178 [hep-ph]].
- [15] A. Alves, E. Ramirez Barreto, and A.G. Dias, Phys. Rev. D **84**, 075013 (2011) [arXiv:1105.4849 [hep-ph]].
- [16] S.-S. Bao, X. Gong, H.-L. Li, S.-Y. Li, and Z.-G. Si, Phys. Rev. D **85**, 075005 (2012) [arXiv:1112.0086 [hep-ph]].
- [17] R. Enberg, R. Pasechnik, and O. Stal, Phys. Rev. D **85**, 075016 (2012) [arXiv:1112.4699 [hep-ph]].

- [18] G.-L. Liu, F. Wang, and S. Yang, Phys. Rev. D **88**, 115006 (2013) [arXiv:1302.1840 [hep-ph]].
- [19] N. Kidonakis, JHEP 05 (2005) 011 [hep-ph/0412422]; Phys. Rev. D **94**, 014010 (2016) [arXiv:1605.00622 [hep-ph]].
- [20] N. Kidonakis, Phys. Rev. D **82**, 054018 (2010) [arXiv:1005.4451 [hep-ph]].
- [21] N. Kidonakis, Phys. Rev. D **77**, 053008 (2008) [arXiv:0711.0142 [hep-ph]].
- [22] N. Kidonakis and A. Sabio Vera, JHEP **02**, 027 (2004) [hep-ph/0311266];  
R.J. Gonsalves, N. Kidonakis, and A. Sabio Vera, Phys. Rev. Lett. **95**, 222001 (2005) [hep-ph/0507317]; N. Kidonakis and R.J. Gonsalves, Phys. Rev. D **87**, 014001 (2013) [arXiv:1201.5265 [hep-ph]]; **89**, 094022 (2014) [arXiv:1404.4302 [hep-ph]].
- [23] N. Kidonakis, in “Physics of Heavy Quarks and Hadrons, HQ2013,” p. 139 [arXiv:1311.0283 [hep-ph]].
- [24] N. Kidonakis, Phys. Rev. D **93**, 054022 (2016) [arXiv:1510.06361 [hep-ph]]; arXiv:1612.06426 [hep-ph].
- [25] N. Kidonakis, Phys. Rev. D **82**, 114030 (2010) [arXiv:1009.4935 [hep-ph]]; **90**, 014006 (2014) [arXiv:1405.7046 [hep-ph]]; **91**, 031501(R) (2015) [arXiv:1411.2633 [hep-ph]].
- [26] G. Sterman, Nucl. Phys. B **281**, 310 (1987).
- [27] S. Catani and L. Trentadue, Nucl. Phys. B **327**, 323 (1989).
- [28] L.A. Harland-Lang, A.D. Martin, P. Molytinski, and R.S. Thorne, Eur. Phys. J. C **75**, 204 (2015) [arXiv:1412.3989 [hep-ph]].
- [29] S. Dulat, T.-J. Hou, J. Gao, M. Guzzi, J. Huston, P. Nadolsky, J. Pumplin, C. Schmidt, D. Stump, and C.-P. Yuan, Phys. Rev. D **93**, 033006 (2016) [arXiv:1506.07443 [hep-ph]].